A Selective Employment of Electronic Effects of the Pentafluorosulfanyl Group Across Linear and Tripodal Push-Pull Chromophores

Michaela Fecková,[a,b] Milan Klikar,[b] Chrisovalantou Vourdaki,[c] Ioannis Georgoulis,[c] Oldřich Pytela,[b] Sylvain Achelle,[d] Zdeňka Růžičková,[e] Mihalis Fakis,[c]* Petr Beier,[f] Filip Bureš[a,b]*

[a] Institute of Technology and Business in České Budějovice, Okružní 517/10, České Budějovice, 37001, Czech Republic

[b] Institute of Organic Chemistry and Technology, Faculty of Chemical Technology, University of Pardubice, Studentská 573, Pardubice, 53210, Czech Republic

[c] Department of Physics, University of Patras, 26500 Greece

[d] Univ Rennes, CNRS ISCR (Institut des Sciences Chimiques de Rennes) UMR 6226, F-35000 Rennes, France

[e] Department of General and Inorganic Chemistry, Faculty of Chemical Technology, University of Pardubice, Studentská 573, Pardubice, 53210, Czech Republic

[f] Institute of Organic Chemistry and Biochemistry, Academy of Sciences of the Czech Republic, Flemingovo nám. 2, Prague, 160 00, Czech Republic

Abstract

Twelve model amino-based linear D-π-A and tripodal D-(π-A)$_3$ chromophores bearing electron-withdrawing SF_5-group(s) at different peripheral positions were designed and prepared in a straightforward way. The influence of the position and the number of SF_5-groups was studied with the aid of single crystal X-ray analysis, thermal and electrochemical measurements, (non)linear steady-state and time resolved spectroscopies, and DFT calculations. Significant property tuning can be achieved when modulating the number and position of the (peripheral) SF_5-group(s), e.g. increase of the thermal robustness from 300 to 420 °C, the HOMO–LUMO gap is tuned through an exclusive manipulation of the LUMO, and the absorption/emission maxima can be red-shifted. The *para*-positioning allowing their hyperconjugation and the increasing number of the appended SF_5-groups along with a polar environment support the intramolecular charge-transfer and open a non-radiative deexcitation channel, while the two-photon absorption cross-section is generally enhanced for the *para*-substituted octupolar chromophores. Thus, properly placing the SF_5-group(s) along the π-conjugated backbone allows a principal tuning of the push-pull chromophore fundamental function(s).

Keywords: pentafluorosulfanyl, push-pull chromophore, negative hyperconjugation, two-photon absorption, electrochemistry.

Introduction

Although the first pentafluorosulfanyl (SF_5) substituted compounds were prepared over six decades ago by W. A. Sheppard,[1] the reported method for oxidizing aryldisulfides by silver difluoride was accompanied by a low yield and variety of side products. These aspects delayed the research interest in pentafluorosulfanyl chemistry for almost forty years, when new synthetic protocols towards SF_5 derivatives were reported by Philp and Umemoto.[2,3] The pentafluorosulfanyl group possesses a very unique combination of properties including thermal and chemical stability as tested by acid/base hydrolysis and pyrolysis.[1] It exhibits both high lipophilicity (e.g. compare Hansch constant π of SF_5 (1.51), CF_3 (1.09), and CN (–0.32) groups) [4] and high electronegativity (e.g. compare Hammett constants σ_p of SF_5 (0.68), CF_3 (0.54), and CN (0.66));[5] the two properties of a chemical moiety that almost never coexist. When comparing the Hammett sigma constants of the cyano group in the *para* and *meta* position (0.66 vs. 0.56), the reduced electron-withdrawing power of the latter is ascribed to a non-resonant arrangement (Figure S1A). However, a similar effect seen for SF_5 (0.68 vs. 0.61) and also CF_3 (0.54 vs. 0.43) is usually explained in terms of a negative hyperconjugation as demonstrated by canonical and no-bond resonance structures (Figure S1B). [6,7] In other words, the electron-withdrawing character of the SF_5 group, which is comparable with that of the cyano group, consists of a strong negative inductive effect and a small resonance contribution via the negative hyperconjugation. These properties make the SF_5 group an attractive substituent, especially when compared to CF_3. Hence, a great number of studies on replacing CF_3 by SF_5 appeared recently, focusing mostly on medicinal applications. [8–10] However, SF_5-substituted organic molecules also found first applications in materials chemistry (Figure 1). [11,12] Examples across organic electronics include self-assembled monolayers of SF_5-terminated oligothioles/sulfides **A** studied as charge transfer materials, [13] SF_5 bearing BODIPY dyes **B** for solar cells, [14,15] charge-transfer polymer **C** used in organic field-effect transistors, [16] and emissive Ir(III) complexes **D** for organic light-emitting diodes. [17] The SF_5-substituted organic and organometallic compounds were also applied as molecular sensors, e.g. redox responsive detector **E**, [18] sensor of mercury(II) ions **D**, [19] and halochromic dye **F**.[20] Substituted pentafluorosulfanylbenzenes **G** have been applied as an energy booster of Li-ion battery catholytes. [21,22] High hydrophobicity of the SF_5 group was utilized in polymer **H** for surface protection coating. [23] We have recently developed a first azo-pyrrole[24] and azo-imidazole[25]

molecular photoswitches **I** bearing pentafluorosulfanyl group on the periphery. It has been demonstrated that bulky SF_5 may stabilize (*Z*)-isomer and thus produce an azo-switch with the half-life exceeding 24 h. Since 2017, the SF_5-group began to be investigated as an electron-withdrawing moiety in push-pull chromophores featuring intramolecular charge-transfer (ICT). The first linear chromophores **J** with *N*,*N*-diphenylamino donor were constructed by Chan et al. [26] as fluorescent and mechanofluorochromic dyes, whose ICT and solvation dynamics were further completed (Figure 1B). [27] Extending the structure of **J** by another one (or two) SF_5-terminated branch(es) afforded quadrupolar (tripodal) triphenylamine-centered chromophores **K,** that utilize the concept of SF_5 negative hyperconjugation to enhance two-photon absorption (2PA) by achieving the 2PA cross-section of 1100–2200 GM.[28] Inspired by these preliminary achievements and as a part of our continuing interest in triphenylamine-based chromophores with 2PA activity, [29–31] we report herein SF_5-caped linear (**1**–**6**) and tripodal (**7**–**12**) push-pull systems (Figure 1C). *N*,*N*-Dimethylamino and triphenylamino groups were utilized as electron donors, while the π-system is modulated by using nonplanar biphenylene and extended/planarized phenylethynylphenyl spacers. Besides the aforementioned *para* substitution in **J** and **K**, utilizing both inductive and resonance effects, we introduce the SF_5 group also in the non-resonant positions *meta* as well as address a cumulation effect of two SF_5 groups. Fundamental chemical, thermal, electrochemical, photophysical, and (non)linear optical properties of **1**–**12** corroborated by quantum-chemical calculations will be discussed.

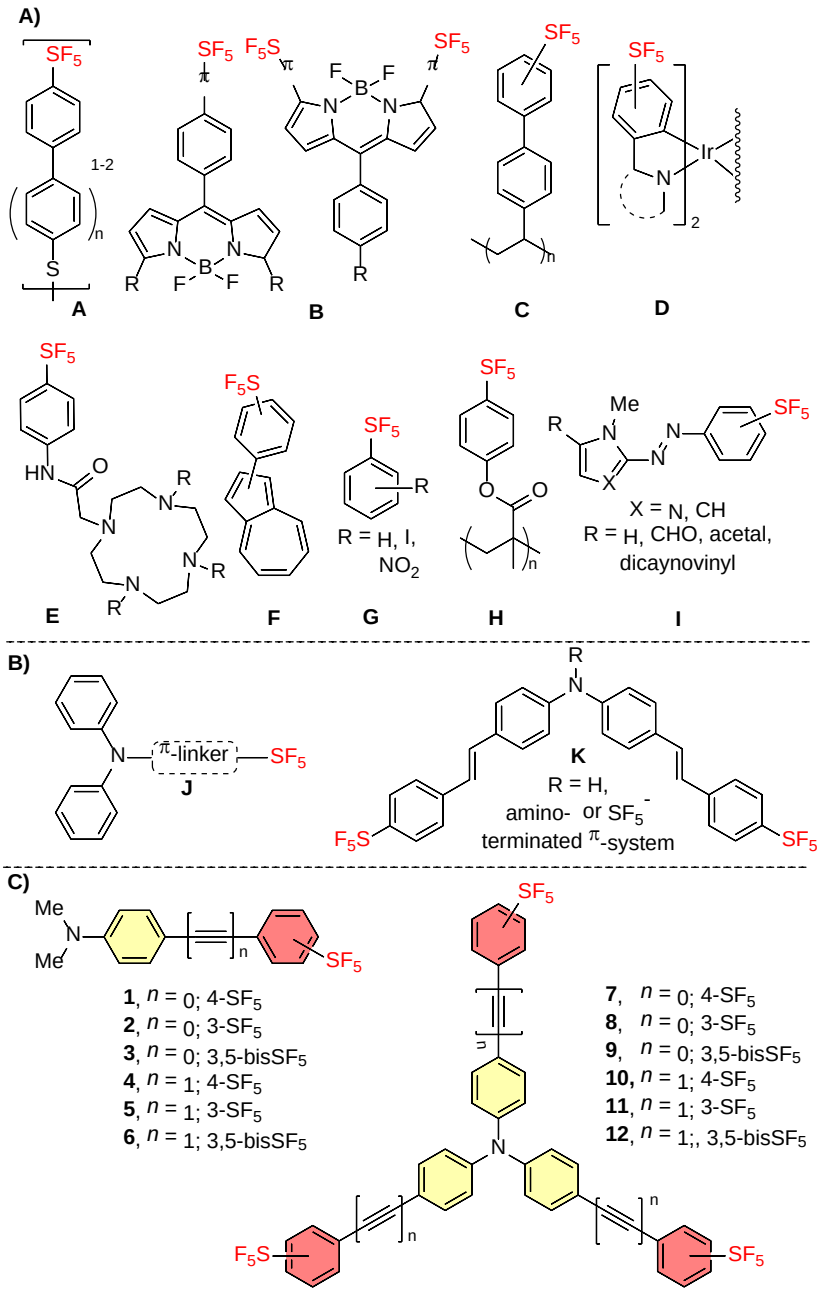

Figure 1. Known organic materials bearing SF_5 group (A), recent push-pull molecules utilizing negative hyperconjugation of the SF_5 group (B), and molecular structure of the investigated chromophores **1**–**12** (C).

Results and Discussion

Synthesis

The linear chromophores **1–3** with biphenyl π-conjugated linker were prepared from 4-(*N*,*N*-dimethylamino)phenylboronic acid and the commercially available halogenated pentafluorosulfanylbenzenes **13a**–**c** using a standard Suzuki-Miyaura cross-coupling reaction (Scheme 1). [32] Analogously, chromophores **4**–**6** with the spacer elongated by an additional acetylenic unit were prepared via a Sonogashira reaction between 4-ethynyl-*N*,*N*-dimethylaniline and **13a**–**c**. [33] Both reactions proceeded smoothly, were accompanied by a

negligible amount of side products (e.g. dehalogenation and homocoupling), and thus afforded the desired products **1**–**6** in high yields (72–88%).

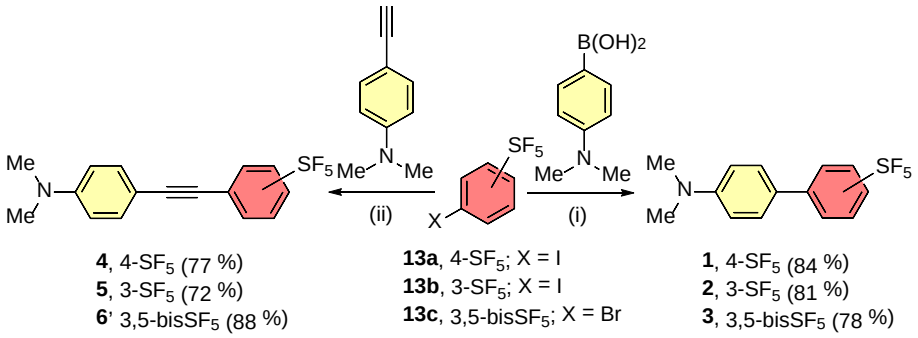

Scheme 1. Synthesis of linear SF_5-capped chromophores **1–6.** (i) $[PdCl_2(PPh_3)_2]$, Na_2CO_3, THF/H_2O (4:1), 60 °C, 16 h; (ii) $[PdCl_2(PPh_3)_2]$, CuI, THF/TEA (4:1), 60 °C, 16 h.

The tripodal derivatives **7**–**12** were synthesized in a similar way by utilizing threefold cross-coupling reactions. The reaction sequence outlined in Scheme 2 involves iodination[34] of triphenylamine and threefold Sonogashira reaction between **14** and trimethylsilylacetylene (TMSA) followed by TMS-group removal affording the terminal acetylene **16** (see the SI for more details). [35] The SF_5-functionalized phenylboronic acid pinacol esters **15a**–**c** were prepared from pentafluorosulfanylbenzenes **13a**–**c** in a one-pot two-steps reaction involving their interconversion to a Grignard reagent using *i*-PrMgCl followed by a reaction with *i*-PrOBpin. Whereas this synthetic strategy afforded **15a**–**c** relatively smoothly, an attempted Miyura borylation[36] or interconversion via organolithium reagents[37] proved unfeasible. Anyway, boronic acid esters **15a**–**c** are unstable intermediates that decompose quickly (see the SI for the native ^{1}H NMR and MS spectra) and, therefore, were used directly in the subsequent Suzuki-Miyaura reaction with **14** furnishing the biphenylene tripodal chromophores **7**–**9** with the yields ranging from 20 to 71%. Starting from **16** and **13a**–**c**, the optimized threefold Sonogashira reaction involving the $[Pd(PPh_3)_4]$ precatalyst and highly-boiling 1,4-dioxane, afforded **10–12** in the yield of 54–78%. As compared to the linear chromophores **1**–**6**, the synthesis of branched chromophores was complicated by a small amount of one/two cross-coupled side products that were separated by column chromatography. Most chromophores exhibit high solubility in common organic solvents due to the presence of the peripheral SF_5-group(s), except **9** and **12** bearing six SF_5-groups that are sparingly soluble in THF and acetone. The low solubility of **9** is also reflected in the low isolated yield. See the SI for more synthetic details and full spectral characterization including native spectra.

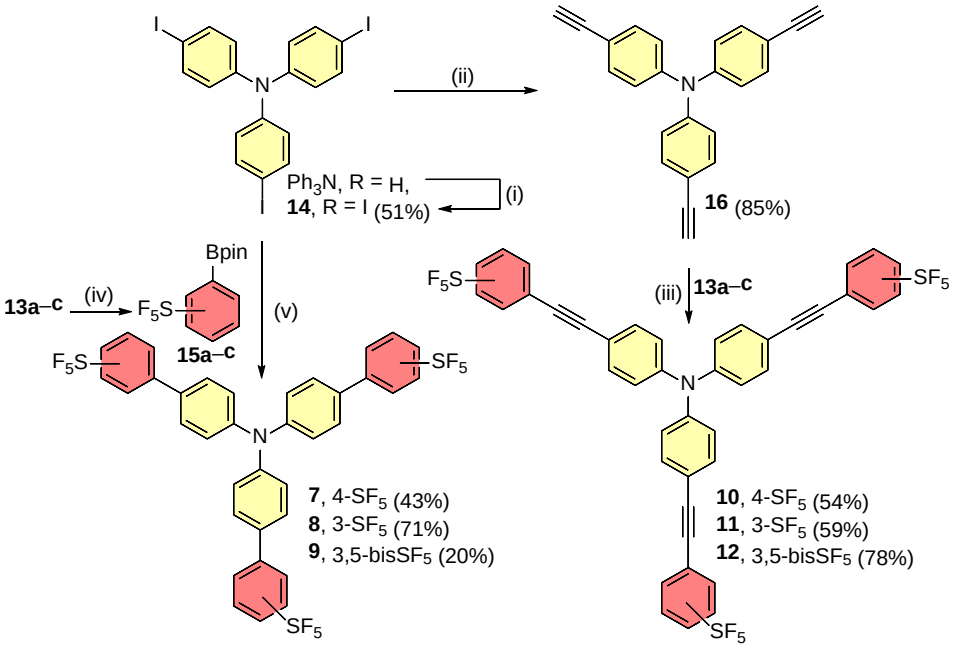

Scheme 2. Synthesis of tripodal final compounds **7–12**. (i) I_2, HgO, EtOH, 25 °C, 24 h; (ii) a: TMSA, $[PdCl_2(PPh_3)_2]$, CuI, THF/TEA (4:1), 60 °C, 36 h; b: K_2CO_3, CH_2Cl_2/EtOH (1:1), 25 °C, 2 h; (iii) $[Pd(PPh_3)_4]$, CuI, 1,4-dioxane/TEA (4:1), 90 °C, 16 h; (iv) a: *i*-PrMgCl, THF, –78 °C, 1 h; b: *i*-PrOBpin, –78→20 °C, 16 h; (v) $[PdCl_2(PPh_3)_2]$, Na_2CO_3, THF/H_2O (4:1), 60 °C, 16 h.

X-ray Analysis

A slow crystallization of chromophores **4**, **5**, and **10** from dichloromethane, hexane or chloroform afforded their single crystals suitable for XRD analysis; Figure 2 shows the obtained ORTEP representations. Whereas **4** and **5** possess relatively planar phenylethynylphenyl spacer with the torsion angle between both appended benzene rings below 10 °, both benzene rings of the same branch in tripodal **10** show rather nonplanar arrangement with the torsion angle of 26 °. This is certainly influenced by the disordered crystal of **10** but also enforced by a typical bowl-shaped arrangement of the central triphenylamine, with the three C-C-N-C torsion angles ranging from 20 to 46 °C. [31,38]

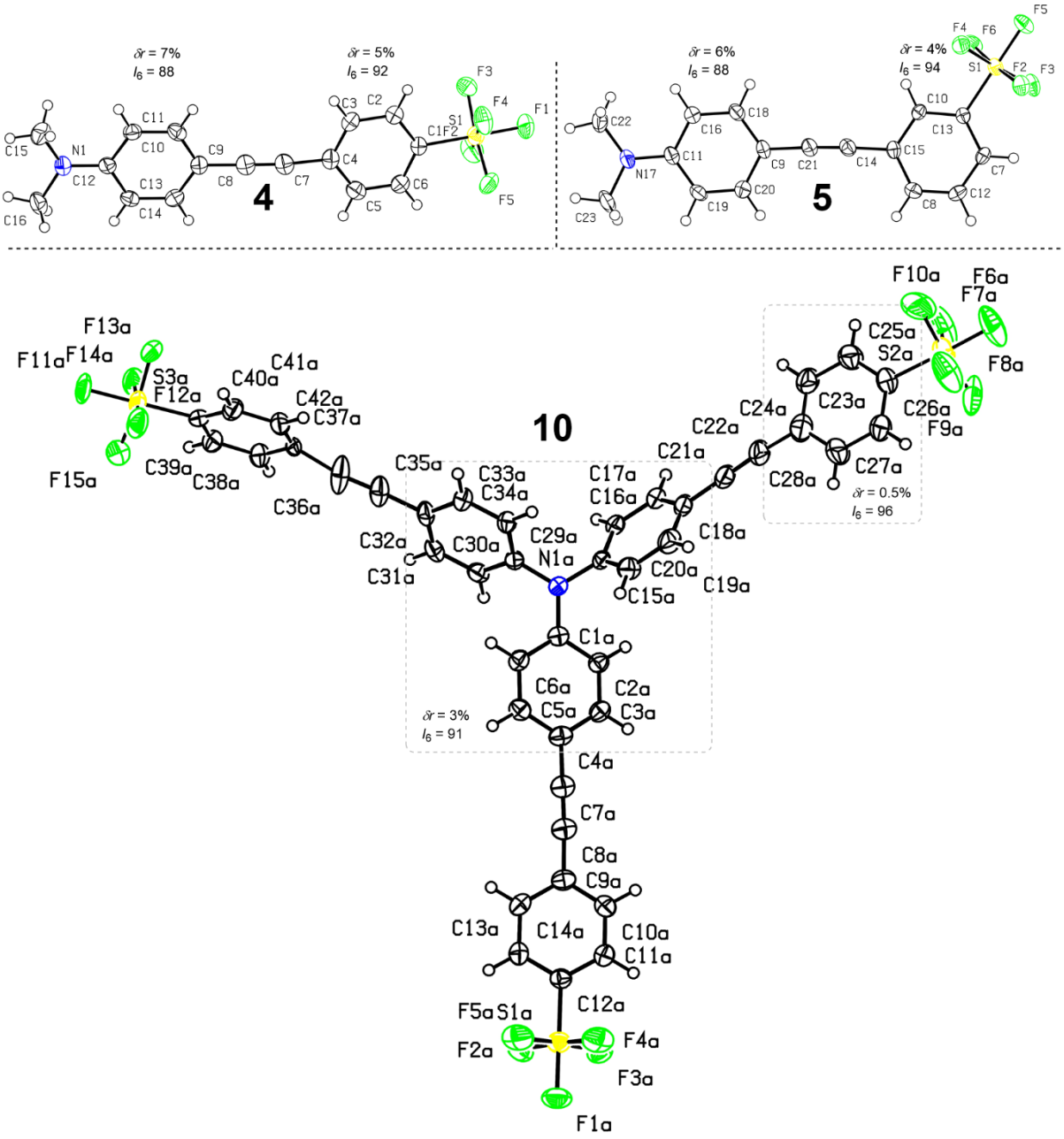

Figure 2. ORTEP representations of chromophores **4** (CCDC 2406744), **5** (CCDC 2406745), and **10** (CCDC 2406746). The hydrogen atoms are shown at the 50% probability level. The quinoid character (δr) and the Bird index (I_6) calculated for the particular benzene rings are further shown.

The SF_5-group(s) adopt(s) a typical octahedral geometry[39] with four equatorial and one axial fluorine atoms and the C-S-F_{ax} moiety nearly coplanar to the appended benzene ring. The F_{ax} and F_{eq} atoms are also distinguishable by ^{19}F NMR spectroscopy (see the experimental part). Whereas the C-S bond length is identical in all crystal structures (1.798 Å), the S-F_{ax} bond length is elongated in **4** (1.584 Å) as compared to **5** (1.581 Å) and **10** (1.577 Å) bearing the SF_5-group in a non-resonant position or when saturated by the weaker triphenylamine central donor. The calculated quinoid character (δr) [40] and the Bird index (I_6) [41,42] of both amino- and

SF_5-substuted benzene rings (Figure 2) imply lower aromaticity of the amino-substituted benzenes (δr = 3–7%, δr in benzene is equal to 0; I_6 = 88–91, I_6 of unsubstituted benzene is equal to 100) compared to the SF_5-substituted rings (δr = 0.5–7%, I_6 = 92–96). When comparing the linear chromophores **4**, **5**, and tripodal **10**, the latter showed a higher degree of aromaticity pointing to a diminished ICT, most probably due to a nonplanar arrangement of the triphenylamine central donor and its lower Hammett constant (compare σ_p = –0.22/–0.83 for Ph_2N- and $(CH_3)_2N$-moieties). The crystal packing of **4** reveals a typical centrosymmetric arrangement for dipolar push-pull chromophores with D-π-A···D-π-A···D-π-A linear chains that are oriented opposite to each other. The chromophore **5** showed rather a herringbone stacking resulting from the *meta*-localization of the SF_5-group. The altering orientation has not been found in the crystal structure of **10**, the tripodal molecules are parallelly aligned with two π-stacked branches and the amino/SF_5 groups oriented in the same way. This results in a weak $F_{eq}\cdots F_{eq}$ van-der-Waals contact (~ 300 pm) of the two neighboring SF_5-groups referred to as type I interaction. [43]

Thermal Properties

The thermal properties of final compounds **1**–**12** were determined by differential scanning calorimetry (DSC) and thermogravimetric analysis (TGA). The melting points (T_m), temperatures of decomposition (T_D), initial temperatures (T_i), and temperatures of 5% mass loss (T_5) are summarized in Tables 1 and S1. Thermograms containing DSC, TGA, and DTG curves (the first derivation of the TGA curve) are provided in the SI (Figure S51–62).

All the investigated compounds exhibited a distinctive endothermic peak of melting followed by an exothermic decomposition process under gradual heating program except tripodal **12**, which decomposed directly without a preceding melting. The biphenylene linear derivatives **1**–**3** decomposed during the evaporation of their liquid phase, while the extended analogues **4**–**6** thermally degraded vigorously prior to evaporation. A complex thermal behavior has been observed for some tripodal molecules. For example, **8** showed a multiple melting process (Figure S58) due to a presence of metastable crystals and a cold crystallization of amorphous **11** was detected between 110–130 °C (Figure S11). When comparing the T_d values (Table 1), the triphenylamine-based chromophores **7**–**12** exhibited higher thermal stability versus the linear analogues **1**–**6**. An elongation of the π-system by an additional acetylenic linker generally reduces the melting point as well as thermal stability, e.g. **2** vs. **5** ($T_{m/d}$ = 122/260 vs. 114/210 °C) or **8** vs. **11** ($T_{m/d}$ = 180/380 vs. 155/280 °C). [30,31,38,44] All the acetylenic derivates **4**–**6** and **10**–**12** decomposed in a multithermal process. The melting point of

compounds bearing the SF_5 group in the *meta*-position is significantly reduced compared to the *para*-substituted analogues, e.g. **1** vs. **2** (T_m = 212 vs. 122 °C) or **10** vs. **11** (T_m = 252 vs. 155 °C). On the contrary, two SF_5 substituents in the *meta*-positions generally increase the melting point in respect to the *meta*-monosubstituted derivatives, e.g. **5** vs. **6** (T_m = 114 vs. 221 °C). When comparing *para*-, *meta*-, and di*meta*-substituted derivatives, e.g. **7** vs. **8** vs. **9** (T_d = 300 vs. 380 vs. 420 °C), the thermal robustness increases considerably. Hence, the tripodal compound **9** based on triphenylamine central scaffold, bearing two *meta*-appended SF_5 groups, and none acetylenic spacer, proved to be the most thermally robust derivative ($T_{m/d}$ = 373/420 °C). TGA measurements carried out in opened crucibles imply that compounds **1**, **6**, and **9** sublime prior to their melting as suggested by the significantly lower T_i and T_5 values compared to T_m (Table S1). This is supported by the isotherms of **1** and **6** showing a linear decrease in weight over time along with none chemical changes seen by ^{1}H NMR (see Figures S63–66 in the SI).

Electrochemistry

The electrochemical behavior of the target chromophores **1–12** was investigated in THF containing 0.1 M Bu_4NPF_6 in a three-electrode cell by cyclic voltammetry (CV). The acquired electrochemical data are summarized in Table 1 (see Figures S67–68 in the SI for the native CV diagrams). Whereas the first oxidations of the biphenylene derivatives **1**–**3** and **7**–**8** are reversible processes, the acetylenic derivatives **4**–**6** and **9**–**12** were oxidized irreversibly. Hence, the anodic peak potential (E_p^{ox1}) has been used to uniformly characterize the oxidation of the whole series. Assuming the first oxidation as one-electron process most likely involving the amino donor, the first reduction was always recorded as fully irreversible multiple-electron transfer characterized by E_p^{red1}. The reduction involves a 3–4 electron process for mono SF_5-substituted derivatives, while the number of exchanged electrons increases when attaching additional SF_5 groups. This behavior corresponds to the previous electrochemical data reported for SF_5-substituted aromatics.[14,45,46] The electrochemical characterization of tripodal derivatives **9** and **12** was complicated by their sparing solubility. The obtained E_p^{ox1} and E_p^{red1} values were further recalculated to the HOMO/LUMO energies ($E_{HOMO/LUMO}$), that are visualized in the energy level diagram (Figure 3A). The steady HOMO level seen for the linear (**1**–**6**) as well as the tripodal chromophores (**7**–**12**) reflects their unaltered electron donor, while the principal changes seen in the energies of the LUMO reflect modifications of the electron acceptor and the π-system. [47] When going from *para* to *meta* SF_5-substituted chromophores, e.g. **1** vs. **2** or **10** vs. **11**), the LUMO became destabilized (ΔE_{LUMO} = +0.04 or +0.17 eV), which

points to a diminished (hyper)conjugation from the non-resonant *meta*-position. However, two SF_5-agroups, despite appended in the *meta*-positions, reduce the E_{LUMO} most significantly (e.g. E_{LUMO} = –2.57, –2.53, and –2.69 eV for **1**, **2**, and **3**). The elongation and planarization by an additional acetylenic spacers bring about a further LUMO stabilization by 0.1–0.2 eV, e.g. E_{LUMO} = –2.57 and –2.70 eV for **1** and **4**. The narrowest HOMO–LUMO gap (ΔE = 2.79 eV) was recorded for chromophore **6** with the linear and planar π-system end-capped by two SF_5-groups. When going from linear to tripodal chromophores, both HOMO and LUMO levels are deepened but the overall ΔE values are slightly increased, e.g. $E_{HOMO/LUMO}$ and ΔE = –2.57/–5.69 and 3.12 eV were recorded for **1** and –2.70/–5.91 and 3.21 eV for **7**. Hence, chromophore branching allows to tune the energies of both frontier molecular orbitals with only diminished effect on the HOMO–LUMO gap, which is consistent with our former conclusions. [44]

The energies of the frontier molecular orbitals were further predicted using DFT B3LYP/6- 311+g(2df,p) method implemented in Gaussian®16W software package. [48] Table 1 lists the calculated values that are further visualized in the energy level diagram (Figure 3A) along with the HOMO/LUMO localization for the two representative chromophores **1** and **12** (Figure 3B); see Figures S77–80 in the SI for the full localizations of the HOMO(–1) and the LUMO(+1) in **1**–**12**. The energy level diagram in Figure 3A shows a very good agreement of the calculated values of the HOMO and slightly overestimated energies of the LUMO compared to the electrochemical data. Importantly, the general trends seen by electrochemistry are obeyed also in the calculated energies. Namely, the position and number of the SF_5-groups, elongation of the π-system, and the arrangement affect mostly the LUMO levels, while the HOMO is relatively steady. Whereas the HOMO is strictly localized on the amino donor, localization of the LUMO varies and reflects positioning of the SF_5-group(s). For *para* SF_5-substituted chromophores **1**, **4**, **7**, and **10**, the LUMO mostly occupies the *para*-position of the SF_5-substituted benzene ring; two branches of tripodal **7** and **10** are involved. The LUMO in (di)*meta* SF_5-substituted linear derivatives extends further to the SF_5 groups, while in tripodal compounds it involves also the conjugated system of the central triphenylamine. This results in a lower HOMO/LUMO separation similarly to that seen for analogous triphenylamine chromophores.[31,38] The HOMO–1 remained on the donor moiety in linear derivatives, whereas it further spreads over one or two branches in tripodal molecules analogously to the LUMO+1, which is a typical feature of $D(-\pi-A)_3$ systems. [29,38] The LUMO and LUMO+1 of **10** and **11** proved to be degenerate.

Table 1. Summarized thermal, electrochemical, optical, and DFT-calculated data of **1–12**.

comp	T_m [°C][a]	T_5 [°C][b]	E_p^{ox1} [V][c]	E_p^{red1} [V][e]	E_{HOMO} [eV][g]	E_{LUMO} [eV][g]	ΔE [eV][h]	E_{HOMO}^{DFT} [eV][i]	E_{LUMO}^{DFT} [eV][i]	ΔE^{DFT} [eV][i]	ΔE^{opt} [eV][j]
1	212	175	1.37[d]	–1.75	–5.69	–2.57	3.12	–5.44	–1.48	3.95	3.78
2	122	152	1.28[d]	–1.79	–5.60	–2.53	3.07	–5.45	–1.52	3.93	3.92
3	131	158	1.38[d]	–1.63[f]	–5.70	–2.69	3.01	–5.63	–2.05	3.58	3.69
4	164	182	1.28	–1.62	–5.60	–2.70	2.90	–5.44	–1.91	3.53	3.48
5	114	180	1.28	–1.74	–5.60	–2.58	3.02	–5.40	–1.74	3.66	3.55
6	221	187	1.33	–1.46	–5.65	–2.86	2.79	–5.56	–2.12	3.43	3.36
7	266	292	1.59[d]	–1.62	–5.91	–2.70	3.21	–5.66	–2.02	3.63	3.44
8	180	323	1.53[d]	–1.68	–5.85	–2.64	3.21	–5.58	–1.85	3.73	3.51
9	373	305	/	–1.55[f]	/	–2.77	/	–5.90	–2.28	3.61	3.42
10	252	376	1.58	–1.48	–5.90	–2.84	3.06	–5.61	–2.38	3.23	3.25
11	155	322	1.55	–1.65	–5.87	–2.67	3.20	–5.54	–2.23	3.31	3.30
12	/	227	/	–1.43[f]	/	–2.89	/	–5.79	–2.62	3.17	3.20

[a] T_m is melting point (the point of intersection of a baseline and a tangent of thermal effect = onset); [b] T_5 is temperature of 5% mass loss (gradual horizontal step on the TGA curve); [c] E_p^{ox1} is anodic peak potential of the irreversible first oxidation process. A low solubility of **9** and **12** makes their E_p^{ox1} values less reliable; [d] Reversible first oxidation; [e] E_p^{red1} is cathodic peak potential of the irreversible first reduction process; [f] Shoulder potential of the first reduction process. All CVs were measured at scan rate 100 mVs^{-1}; all potentials are given vs. Ag/AgCl electrode (SSCE); [g] $-E_{HOMO/LUMO}$ = (E_p^{ox1} + 0.036) or (E_p^{red1} + 0.036) + 4.28 (vs. SCE). [49,50] The increment of +0.036 V corresponds to the difference between SCE (0.241 vs. SHE) and SSCE (0.205 vs. SHE)); [51] [h] Electrochemical HOMO–LUMO gap: $\Delta E = E_p^{ox1} - E_p^{red1}$; [i] Energies of the frontier molecular orbitals and their difference were calculated at the DFT B3LYP/6-311++g(2df,p) level of theory in toluene; [j] Optical gap calculated from the experimentally measured absorption maxima in toluene using the equation: ΔE^{opt} [eV] = 1240 / λ_{max}^{A} [nm].

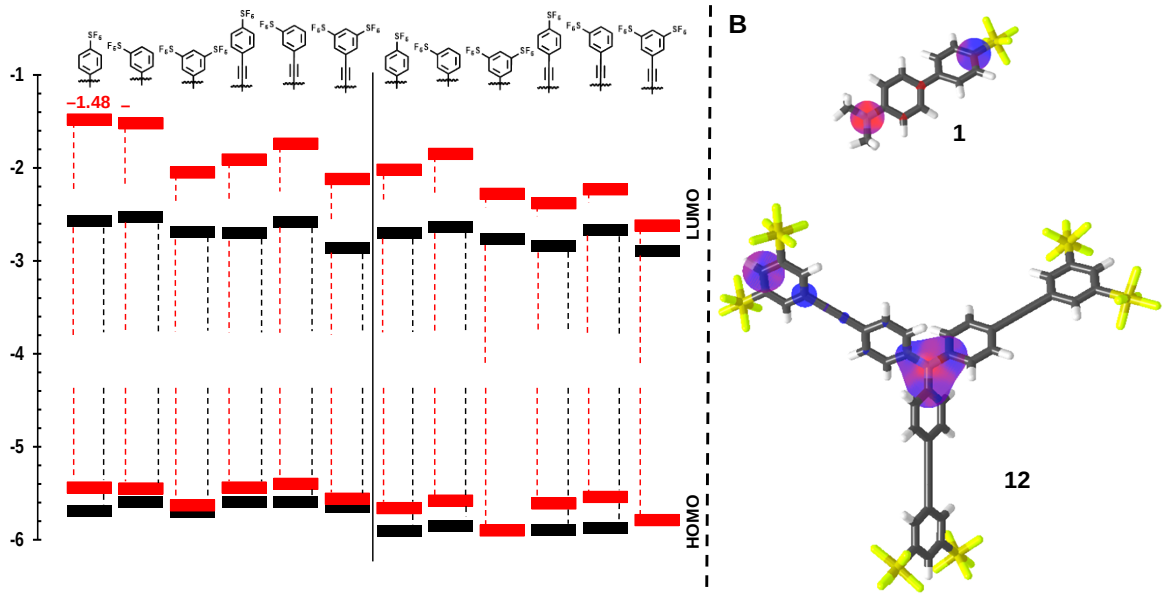

Figure 3. Energy level diagram of chromophores **1–12** showing electrochemical (black) and DFT-calculated (red) energies of the frontier molecular orbitals (A) and the HOMO (red) and the LUMO (blue) localizations in representative chromophores **1** and **12**.

Linear Optical Properties

The fundamental optical properties of chromophores **1–12** were investigated in solvents of various polarity including *n*-heptane (HEPT), toluene (TOL), tetrahydrofuran (THF), dichloromethane (DCM), and acetone (ACT), see Table S2 and Figures S69–75 in the SI. Photophysical data measured in toluene are provided in Table 2 along with the emission maxima

in the solid state (powder), and the DFT calculated absorption maxima. The absorption and emission spectra in toluene are displayed in Figure 4.

Table 2. The longest wavelength absorption maxima (λ_{max}^{A}), the molar absorption coefficients at the absorption maxima (ε), the fluorescence emission maxima (λ_{max}^{E}), and the fluorescence quantum yields (Φ_F) of chromophores **1–12** measured in toluene along with the emission maxima in the solid state and the calculated absorption maxima.

	Solution			Solid state	Predicted
comp	λ_{max}^{A} [nm] (ε [×10^3 M^{-1}·cm^{-1}])[a]	λ_{max}^{E} [nm][a]	Φ_F[b]	λ_{max}^{E} (powder) [nm]	λ_{max}^{A} (DFT)[c] [nm]
1	328 (23.1)	391, 407	<0.01	403	348
2	316 (21.9)	410, 435	<0.01	438	322
3	336 (20.0)	410, 435	<0.01	394	357
4	356 (30.4)	412	0.09	451	390
5	349 (28.0)	390	0.03	419	376
6	369 (28.0)	430	0.01	468	399
7	360 (50.6)	410	0.71	435	397
8	353 (50.2)	400	0.59	442	385
9	362 (14.6)[d]	413	0.48	423	399
10	381 (77.9)	418	0.88	468	399
11	376 (75.8)	410	0.76	451	441
12	387 (15.8)[d]	423	0.78	511	451

[a] The spectra were recorded in toluene at $c = 1 \pm 0.1 \times 10^{-5}$ M at 20 °C. [b] Fluorescence quantum yield (±10%) determined relative to 1,4-bis(5-phenyl-2-oxazolyl)benzene in cyclohexane (Φ_F = 0.975).[52] [c] The absorption maxima calculated at the DFT B3LYP/6-311++g(2df,p) in toluene. [d] Low solubility.

The absorption spectra (Figure 4) of both linear and tripodal chromophores **1**–**12** feature one single band with the longest wavelength absorption maxima appearing between 316 and 387 nm, which can be attributed to a charge-transfer band. Its position depends on the localization and number of SF_5-group(s) as well as composition of the π-linker. When comparing the localization of the SF_5-group(s), the most bathochromically shifted λ_{max}^{A} values were recorded for 3,5-bisSF_5-substituted chromophores followed by *para* and *meta* derivatives, e.g. λ_{max}^{A} = 336, 328, and 316 nm for **3**, **1**, and **2**). Hence, the electron-withdrawing power of the SF_5-group consists of resonance contribution (negative hyperconjugation) and strong inductive effect that can be selectively employed. Approximately 20–30 nm red-shift can be induced upon inserting an additional acetylenic unit (biphenylene→phenylethynylphenyl linkers), e.g. λ_{max}^{A} = 328/356 and 360/381 nm for **1**/**4** and **7**/**10**. These outcomes are in line with the electrochemical measurements. The absorption spectra of tripodal chromophores **7**–**12** (Figure 4C/D) feature a single band without any splitting, which can be explained in terms of Frenkel exciton model generally predicting three excited states. However, the two low-energy lying states (as to the corresponding linear chromophore) are degenerated, while the high-energy lying state has zero oscillator strength.[53] When compared to the corresponding linear analogues **1**–**6**, this accounts for the slightly red-shifted single band seen for **7**–**12** ($\Delta\lambda_{max}^{A}$ ~ +30 nm). The other trends are similar to those observed for linear chromophores. The molar absorption coefficient at λ_{max}^{A} is primarily influenced by the π-linker extension, e.g. a growth

of ε is seen in the order of **1** (23.1) < **4** (30.4) < **7** (50.6) < **10** (77.9×10^3 M^{-1}·cm^{-1}). A very minor solvatochromic effect on the longest wavelength absorption maxima was observed when changing the solvent, which is a typical feature of push-pull chromophores. [47] The TD-DFT calculated absorption spectra overlapped with the experimental ones are presented in Figures S81–82, while the calculated longest-wavelength absorption maxima (λ_{max}^{A}(DFT)) and the corresponding optical gaps (ΔE^{opt}) are listed in Tables 2 and 1. Despite slightly red-shifted, the calculated spectra feature the same number of bands and shape compared to the experimental ones and the predicted longest-wavelength absorption maxima and the HOMO–LUMO gaps correlate tightly with the experimental values (Figures S83–84). The longest wavelength band of biphenylene chromophores **1**–**3** is generated by the transition(s) from the HOMO to the LUMO+1 and/or the LUMO+2, while a sole HOMO→LUMO transition has been revealed for planarized and extended chromophores **4**–**6**. The absorption band of all tripodal derivatives **7**–**12** consists of the HOMO→LUMO and the HOMO→LUMO+1 transitions.

Analogously to the absorption, the emission spectra of **1**–**12** (Figure 4) comprise of a single band appearing between 364 and 504 nm (Table 2). In general, the emission intensity increases with enlarging the π-system, while the position of the emission maxima (λ_{max}^{E}) is influenced by the number and position of the appended SF_5-groups similarly to the trends seen in the absorption spectra. A small bathochromic shift in λ_{max}^{E} is also observed when extending the π-system. The fluorescence quantum yield is mostly affected by the used solvents (Table S2). The linear chromophores **1**–**6** are weakly emissive in nonpolar HEPT and TOL ($\Phi_F \leq 0.14$) and practically none emission is seen in more polar THF, DCM, and ACT. The tripodal chromophores **7**–**12** are highly emissive in TOL and HEPT (Φ_F = 0.33–0.88), while their emissive behavior is suppressed in the solvents of higher polarity. The positive emission solvatochromism indicates higher dipole moment of the excited state, compared to the ground state. The more polar solvents stabilize the polar excited state, which results in an increasing Stokes shift (1600 to 8660 cm^{-1}; Table S2). The large Stokes shift values in polar solvents also point to a significant structural rearrangement of chromophores upon excitation. The excited state stabilization by polar solvents also promotes non-radiative decays leading to a significant decrease in the emission intensity (Tables S2). [54,55] The emission maxima plotted against the Dimroth-Reichardt polarity parameter E_T (30) (Figure S76) indicates that the SF_5-group positioned in the *para* position impart a stronger ICT compared to the *meta*-substituted analogues. However, two *meta*-positioned SF_5-groups polarize the π-system even strongly. This trend is especially pronounced across planar phenylethynylphenyl π-linker. The chromophores

7 and **10** can be further compared to an analogous tripodal derivative bearing stilbenyl π-linker reported by Chan et al. ($\lambda_{max}^{A/E}$ = 409/482 nm, Φ_F = 0.49 in $CHCl_3$). [56] The red-shifted $\lambda_{max}^{A/E}$ values of the latter reflect a more efficient ICT across the stilbenyl π-linker as compared to biphenylene and phenylethynylphenyl ones, which is in line with the fundamental principles of the property tuning in push-pull molecules. [47]

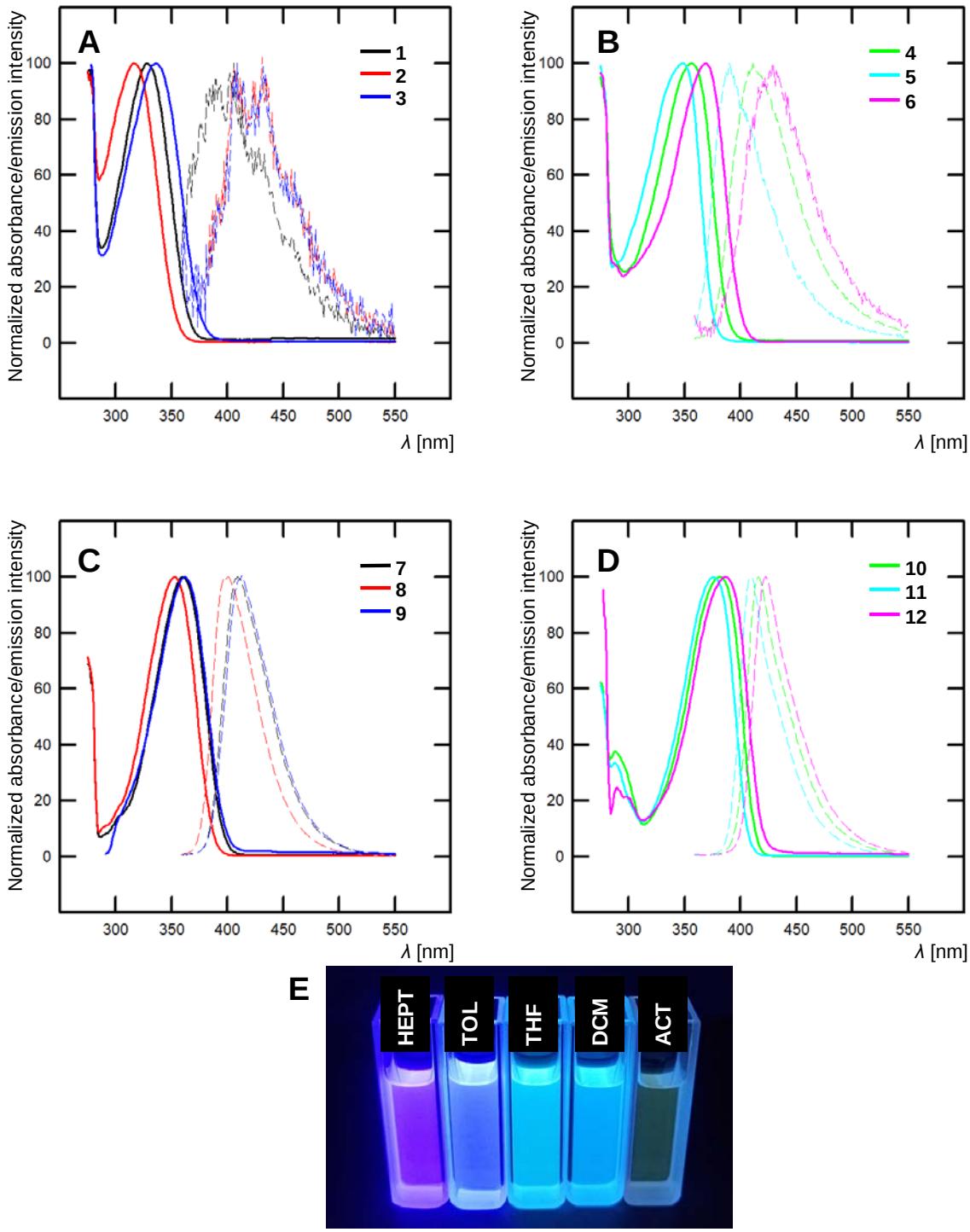

Figure 4. Normalized absorption (solid lines) and emission spectra (dashed lines) of chromophores **1–3** (A), **4–6** (B), **7–9** (C), and **10–12** (D) in toluene at $c = 1 \pm 0.1 \times 10^{-5}$ M. Photograph of solutions of chromophore **12** under irradiation with UV lamp (λ_{em} = 254 nm) (E).

The emission spectra of powdered chromophores measured at room temperature (Figure 5 and Table 2) reveal dark blue emission (λ_{max}^{E} = 394–468 nm) for the linear chromophore **1–6**, whereas tripodal chromophores **7**–**11** exhibit light blue emission (λ_{max}^{E} = 423–468 nm). The most extended chromophore **12** with six peripheral SF_5-groups possesses the most red-shifted emission maxima in the green region (λ_{max}^{E} = 511 nm). Compared to the emission in the solution, the emission maxima of all chromophores are significantly red-shifted in the solid state, which points to a significant intermolecular interaction and an eventual formation of excimers as also suggested by the aforementioned XRD data.

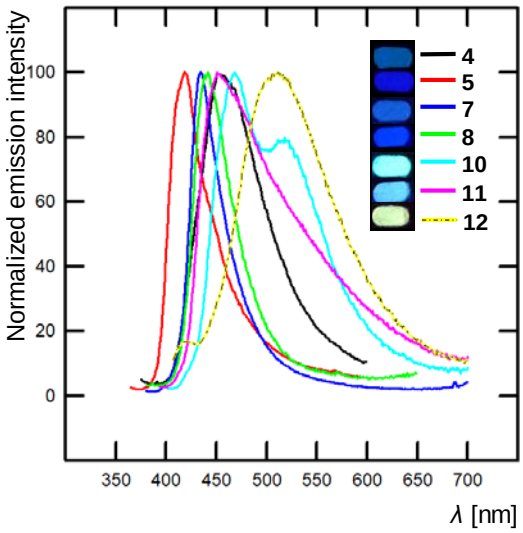

Figure 5. Normalized emission spectra of compounds **4**, **5**, **7**, **8**, and **10–12** in the solid state. Photographs of the solid-state samples under UV lamp irradiation (λ_{em} = 254 nm) are shown as an inset.

Time resolved spectroscopy

As a further step, the role of the position and the number of SF_5-group(s) in the excited state dynamics has been studied. The molecules **10–12** have been examined since they exhibit emission in the visible spectrum with high Φ_F values. Figure 6 shows the fluorescence decays in three solvents on the ns timescale, while Table S3 summarizes the fitting data. The observed bi-exponential behavior points to the existence of two decay mechanisms, which can be explained by considering two emission states, the locally excited (LE) state and the state populated after ICT. The latter is favored, because of the push-pull nature of **10**–**12**, possesses a longer lifetime, and prevails in polar environments. In TOL, all three chromophores show similar average lifetimes of about 1.3 ns. In THF, mono-substituted chromophores **10** and **11** showed slightly increased lifetimes due to an increased contribution of the ICT state. On the contrary, the lifetime of **12** in THF decreased, most probably due to a strengthening of a non-radiative mechanism caused by six peripheral SF_5 acceptors. In the most polar ACT, a non-

radiative mechanism is operational for all chromophores, which results in considerably decreased lifetimes. The lifetime of **12** in ACT is an order of magnitude smaller compared to that in TOL, which correlates with the highest number of the *meta*-placed SF_5-groups. Comparing **10** and **11**, the lifetime decreases more significantly for the former, which relates to a stronger ICT towards the *para*-placed SF_5-group. These findings agree with the increased Stokes shift of **12** and **10** compared to **11** and to the measured Φ_F values.

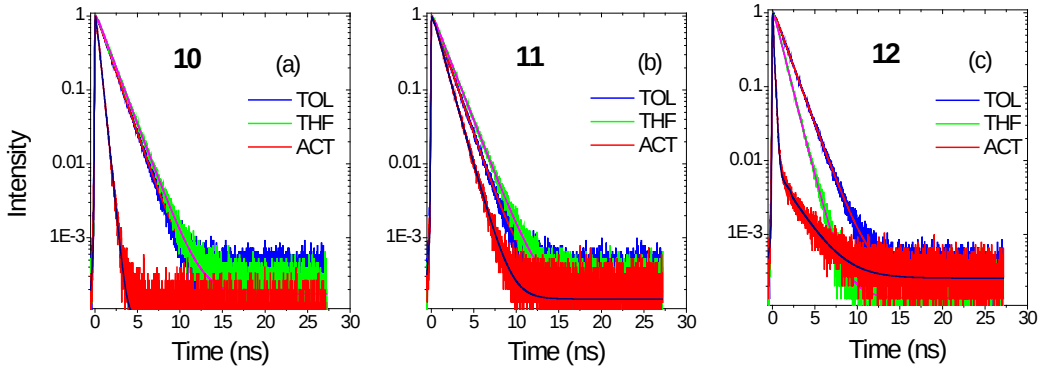

Figure 6. Fluorescence dynamics in the ns timescale for (a) **10**, (b) **11** and (c) **12** in TOL, THF and ACT, exc.: 400 nm, det.: at the peaks of the emission spectra.

Since occurring within the timescales of 100 fs–10 ps, the aforementioned time-resolved fluorescence measurements in the ns timescale do not provide information about the fast relaxation phenomena such as solvation, vibronic relaxation, energy transfer, and how the charge is distributed in the excited state. Thus, we also performed time-resolved measurements via the femtosecond up conversion (FU) technique in TOL and THF for the molecules **10** and **11** (**12** provided a very low signal). Measurements were made at an excitation wavelength of 380 nm, i.e close to the absorption peaks, while the decays were recorded at different emission wavelengths. Figure 7 shows the dynamics for the first tens of ps at different detection wavelengths. In TOL, the fluorescence intensity of the samples for all detection wavelengths is almost constant for the first 50 ps, which means that there is no relaxation and ICT state population of the excited state in non-polar TOL. This contrasts to THF, where the fluorescence dynamics shows a fast decay at short wavelengths and a slow increase in the fluorescence intensity for the longer ones. This phenomenon is explained by the fact that the molecules undergo solvent relaxation as well as energy transfer from the initially excited state to a lower energy ICT state and therefore the emission is gradually shifted to longer wavelengths. [57–62] For the analysis of the excited state dynamics, a global fitting method was used and two decay times were found for each chromophore while a third component corresponding to the excited state lifetime (obtained by the TCSPC technique) was also used. These results are shown in Table 3. In THF, chromophore **10** has a faster decay than **11** and this is associated with more

efficient ICT towards the *para*-positioned SF_5-group. Specifically, **10** exhibits relaxation times of 0.28 ps and 2.34 ps, while the relaxation of **11** occurs via 0.72 ps and 3.37 ps. The first time is slightly slower than the solvation time for THF, while the second mechanism can be related to slower relaxation processes such as diffusion solvation and ICT population.[63,64] *meta*-Substituted chromophore **11** exhibits slower times, as the polarity of their excited state is lower than that of **10** bearing the SF_5-group in the *para* position.

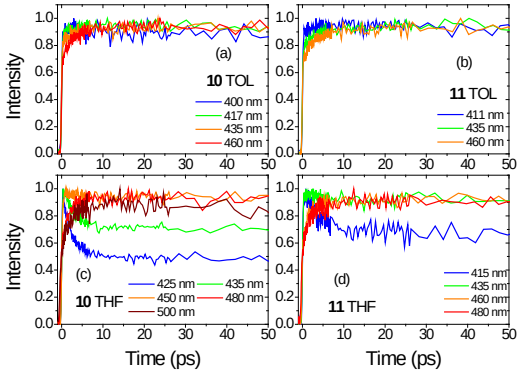

Figure 7. Fluorescence up conversion dynamics in the ps timescale in TOL for (a) **10** and (b) **11** and in THF for **10** (c) and **11** (d) exc.: 380 nm, det.: at various emission wavelengths as shown in the figure.

Table 3. Fitting results of the fluorescence up conversion dynamics for **10** and **11** in TOL and THF. A third decay mechanism was also used with lifetime equal to the ns decay time found by the TCSPC method (not shown).

comp	Solvent	λ_{det}(nm)	A_1	τ_1(ps)	A_2	τ_2(ps)
10	TOL	400	-0.11	0.87	0.04	4.25
		417	-0.03		-0.06	
		435	-0.06		-0.09	
		460	-0.12		-0.19	
	THF	425	0.11	0.28	0.49	2.34
		435	-0.19		0.36	
		450	-0.33		0.03	
		480	-0.52		-0.36	
		500	-0.40		-0.43	
11	TOL	411	-0.07	1.88	-0.005	13.4
		435	-0.13		-0.09	
		460	-0.19		-0.11	
	THF	415	-0.11	0.72	0.34	3.37
		435	-0.06		0.07	
		460	-0.30		-0.16	
		480	-0.33		-0.22	

Fluorescence anisotropy measurements were also performed on the fs time scale using the FU technique (Figure 8). Information will be mainly obtained from the initial value of the anisotropy and fast depolarization time and not from the rotational time since rotation is a slow phenomenon exceeding 100 ps. The solvents used were TOL and THF. In TOL, **10** and **11** have initial anisotropies of approximately 0.15 and 0.18 while in THF larger values of 0.25 and 0.24 were found. Besides, the initial stage of depolarization takes place on the 1–10 ps timescale, being more obvious for THF. The fitting results are listed in Table S4. These values of the initial anisotropy as well as the initial fast decay, leading to an anisotropy of approximately 0.1, are

expected for octupolar molecules. [65–68] The sharp decrease in the anisotropy in the first few ps can be explained by an energy redistribution phenomenon, [69] implying an energy transfer between branches either through a bond (coherent energy transfer) or through a space (incoherent energy transfer). The measured anisotropy decay times are consistent with the incoherent energy transfer. [70] A missing anisotropy decay on the 10–100 fs scale, which would correspond to a coherent transfer, is probably related to a course faster than the IRF of this system.

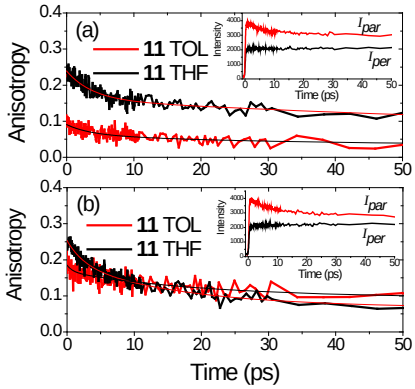

Figure 8. Time resolved anisotropy dynamics in the ps timescale for **10** and **11** in TOL and THF, exc.: 380 nm, det.: at the peak of the emission spectra. The insets show the fluorescence dynamics detected at a parallel and perpendicular polarization for **10** (a) and **11** (b) in THF respectively.

Two-Photon Absorption

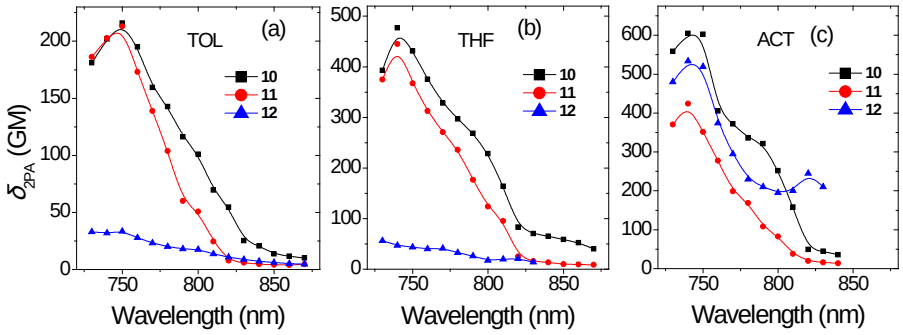

Figure 9. 2PA spectra for **10**, **11**, and **12** in TOL, THF, and ACT.

The 2PA spectra of **10**–**12** were studied in TOL, THF, and ACT (Figure 9). In TOL and THF, the largest 2PA cross-section values (δ_{2PA} reaching ca. 450 GM in THF at 740 nm) were measured for the isomeric chromophores **10** and **11**. Chromophore **12** with two SF_5 acceptors per branch showed significantly diminished cross-section of ca. 60 GM. Hence, although enhances the ICT, the second SF_5-group in **12** leads to a decrease of the 2PA cross section values within our spectral range. However, in more polar ACT, *para*- and di*metha*-substituted

chromophore **10** and **12** showed enhanced 2PA cross-sections with values of ca. 500–600 GM, which is a consequence of the greatly reduced Φ_F values.

Conclusion

Twelve novel chromophores bearing *N*,*N*-dimethylamino or triphenylamine electron donors interconnected to one or two peripheral SF_5-group(s) via biphenylene or phenylethynylphenyl π-conjugated spacers were prepared by mono- or threefold Suzuki-Miyaura or Sonogashira cross-coupling reactions. The X-ray analysis revealed that the axial S-F bond of the SF_5-group is elongated with the more pronounced ICT pointing to an increased negative hyperconjugation. The appended SF_5-groups also significantly affect the supramolecular arrangement in the solid state. The thermal robustness of the synthesized chromophores is dictated by inclusion of the acetylenic linker as well as the number of peripheral SF_5-groups. When comparing *para*-, *meta*-, and di*meta*-substituted chromophores, the thermal robustness increased considerably (300 to 420 °C). Whereas the HOMO is localized on the amino donor, the LUMO spreads over the peripheral benzene ring bearing the SF_5-group(s). Altering the number and position of the SF_5-groups allows tuning of the HOMO–LUMO gap exclusively via manipulating the LUMO. The hyperconjugation of SF_5 is suppressed from the non-resonant *meta*-position compared to *para*, but the most deepened LUMO is achieved with the two *meta*-positioned SF_5-groups. The 3,5-biSF_5-substituted chromophores also possess the most red-shifted absorption maxima, followed by that of *para*- and *meta*-derivatives. When going from linear to tripodal chromophores, the molar absorption coefficient can be significantly tuned from 20 to 80×10^3 $M^{-1}\cdot cm^{-1}$ as a result of the π-system elongation. Analogously to the absorption properties, the number and position of the SF_5-groups also affect the emission behavior. The emission is intensive in nonpolar solvents and reduces with increasing the solvent polarity, pointing to a more polar excited state, as also seen by gradually increasing Stokes shift (1500 to 8600 cm^{-1}). Compared to solution, the emission maxima of all push-pull chromophores are red-shifted in the solid state, which implies a significant intermolecular interaction ($\Delta\lambda_{max}^{E}$ = 70–120 nm). The time resolved spectroscopy of selected tripodal molecules revealed locally excited and ICT states, the latter becomes significantly operative in polar solvents. The increasing number of appended SF_5-groups or their hyperconjugation from the resonant positions as well as a polar environment open a non-radiative (ICT) channel as confirmed by femtosecond up conversion technique. Fluorescence anisotropy measurements of tripodal chromophores further pointed to an incoherent energy transfer between branches. The aforementioned spectral properties are further reflected in the

experimentally measured 2PA cross-sections that are generally higher for *para*-substituted tripodal chromophores, but can be significantly enhanced in polar solvents for di*metha*-derivative. The SF_5-group positioned in the *para* position impart a stronger ICT compared to the *meta*-substituted analogues. However, depending on the environment, two *meta*-positioned SF_5 groups polarize the π-system even strongly. In summary, attaching SF_5-group to a conjugated system brings about increased thermal resistance and solubility, polarization through σ- and π-bonds, altered supramolecular arrangement, and most importantly tunable optical properties and FMOs. The latter property is especially important for organic electronic.

Supporting Information Summary

Full experimental details and characterization are provided in the Supporting Information file. Deposition Numbers 2406744 (for **4**), 2406745 (for **5**), and 2406746 (for **10**) contain the supplementary crystallographic data for this paper. These data are provided free of charge by the joint Cambridge Crystallographic Data Centre. The authors have cited additional references within the Supporting Information.[71–79]

Acknowledgements

MF and FB are indebted to the Specific University Research project "Study of material properties and production technologies within the Environmental Research Department" (No. 07SVV2325) mediated by the Ministry of Education, Youth and Sports of the Czech Republic. MF, MK, OP, and FB acknowledge the support from the European Regional development Fund-Project "Innovative materials with high added value suitable for applications (INMA)", No. CZ.02.01.01/00/23_021/0008593.

PB is indebted to the Czech Academy of Science (Research Plan RVO: 61388963).

Conflict of Interest

The authors declare no conflict of interest.

Data Availability Statement

The data that support the findings of this study are available from the corresponding author upon reasonable request.

References

[1] W. A. Sheppard, *J. Am. Chem. Soc.* **1962**, *84*, 3064–3072.

[2] R. D. Bowden, P. J. Comina, M. P. Greenhall, B. M. Kariuki, A. Loveday, D. Philp, *Tetrahedron* **2000**, *56*, 3399–3408.

[3] T. Umemoto, L. M. Garrick, N. Saito, *Beilstein J. Org. Chem.* **2012**, *8*, 461–471.

[4] Corwin. Hansch, R. M. Muir, Toshio. Fujita, P. P. Maloney, Fred. Geiger, Margaret. Streich, *J. Am. Chem. Soc.* **1963**, *85*, 2817–2824.

[5] C. Hansch, A. Leo, R. W. Taft, *Chem. Rev.* **1991**, *91*, 165–195.

[6] W. A. Sheppard, *J. Am. Chem. Soc.* **1962**, *84*, 3072–3076.

[7] O. Exner, S. Böhm, *New J. Chem.* **2008**, *32*, 1449–1453.

[8] S. Altomonte, M. Zanda, *J. Fluorine Chem.* **2012**, *143*, 57–93.

[9] D. Barnes-Seeman, J. Beck, C. Springer, *Curr. Trends Med. Chem.* **2014**, *14*, 855–864.

[10] M. Sani, M. Zanda, *Synthesis* **2022**, *54*, 4184–4209.

[11] J. M. W. Chan, *J. Mater. Chem. C* **2019**, *7*, 12822–12834.

[12] R. Kordnezhadian, B.-Y. Li, A. Zogu, J. Demaerel, W. M. De Borggraeve, E. Ismalaj, *Chem. Eur. J.* **2022**, *28*, e202201491.

[13] Y. Liu, M. Zeplichal, S. Katzbach, A. Wiesner, S. Das, A. Terfort, M. Zharnikov, *Nano Res.* **2023**, *16*, 7991–8002.

[14] R. D. James, L. S. Alqahtani, J. Mallows, H. V. Flint, P. G. Waddell, O. J. Woodford, E. A. Gibson, *Sustainable Energy Fuels* **2023**, *7*, 1494–1501.

[15] R. D. James, F. Cucinotta, P. G. Waddell, A. C. Benniston, *New J. Chem.* **2023**, *47*, 8451–8459.

[16] G. Zhang, Y.-J. Lee, P. Gautam, C.-C. Lin, C.-L. Liu, J. M. W. Chan, *J. Mater. Chem. C* **2019**, *7*, 7865–7871.

[17] N. M. Shavaleev, G. Xie, S. Varghese, D. B. Cordes, A. M. Z. Slawin, C. Momblona, E. Ortí, H. J. Bolink, I. D. W. Samuel, E. Zysman-Colman, *Inorg. Chem.* **2015**, *54*, 5907–5914.

[18] R. T. Kadakia, R. T. Ryan, D. J. Cooke, E. L. Que, *Chem. Sci.* **2023**, *14*, 5099–5105.

[19] X.-F. Ma, X.-F. Luo, Z.-P. Yan, Z.-G. Wu, Y. Zhao, Y.-X. Zheng, J.-L. Zuo, *Organometallics* **2019**, *38*, 3553–3559.

[20] S. J. Webster, C. M. López-Alled, X. Liang, C. L. McMullin, G. Kociok-Köhn, C. L. Lyall, T. D. James, J. Wenk, P. J. Cameron, S. E. Lewis, *New J. Chem.* **2019**, *43*, 992–1000.

[21] A. R. Sevilla, H. Gao, K. J. Steinberg, B. M. Gallant, *J. Phys. Chem. C* **2023**, *127*, 1722–1732.

[22] H. Gao, A. R. Sevilla, G. M. Hobold, A. M. Melemed, R. Guo, S. C. Jones, B. M. Gallant, *Proc. Natl. Acad. Sci. U.S.A.* **2022**, *119*, e2121440119.

[23] Y. Xie, J. Iwata, T. Matsumoto, N. L. Yamada, F. Nemoto, H. Seto, T. Nishino, *Langmuir* **2022**, *38*, 6472–6480.

[24] V. Jelínková, A. Dellai, L. Verwaerde, V. Rodriguez, M. Fecková, M. Vachtlová, J. Podlesný, M. Klikar, B. Sempé, M. Hugget, P. Pařík, O. Pytela, F. Castet, Z. Růžičková, F. Bureš, *Chem. Eur. J.* **2025**, *31*, e202404221.

[25] V. Jelínková, A. Dellai, M. Vachtlová, M. Fecková, J. Podlesný, M. Klikar, F. Castet, A. Růžička, P. Pařík, O. Pytela, F. Bureš, *J. Photochem. Photobiol., A* **2024**, *449*, 115390.

[26] P. Gautam, C. P. Yu, G. Zhang, V. E. Hillier, J. M. W. Chan, *J. Org. Chem.* **2017**, *82*, 11008–11020.

[27] X. Niu, P. Gautam, Z. Kuang, C. P. Yu, Y. Guo, H. Song, Q. Guo, J. M. W. Chan, A. Xia, *Phys. Chem. Chem. Phys.* **2019**, *21*, 17323–17331.

[28] P. Gautam, Y. Wang, G. Zhang, H. Sun, J. M. W. Chan, *Chem. Mater.* **2018**, *30*, 7055–7066.

[29] D. Cvejn, E. Michail, I. Polyzos, N. Almonasy, O. Pytela, M. Klikar, T. Mikysek, V. Giannetas, M. Fakis, F. Bureš, *J. Mater. Chem. C* **2015**, *3*, 7345–7355.

[30] M. Klikar, K. Seintis, I. Polyzos, O. Pytela, T. Mikysek, N. Almonasy, M. Fakis, F. Bureš, *ChemPhotoChem* **2018**, *2*, 465–474.

[31] M. Klikar, D. Georgiou, I. Polyzos, M. Fakis, Z. Růžičková, O. Pytela, F. Bureš, *Dyes Pigm.* **2022**, *201*, 110230.

[32] N. Miyaura, T. Yanagi, A. Suzuki, *Synth. Commun.* **1981**, *11*, 513–519.

[33] K. Sonogashira, *J. Organomet. Chem.* **2002**, *653*, 46–49.

[34] O. P. Varnavski, J. C. Ostrowski, L. Sukhomlinova, R. J. Twieg, G. C. Bazan, T. Goodson, *J. Am. Chem. Soc.* **2002**, *124*, 1736–1743.

[35] P.-Z. Li, X.-J. Wang, S. Y. Tan, C. Y. Ang, H. Chen, J. Liu, R. Zou, Y. Zhao, *Angew. Chem., Int. Ed.* **2015**, *54*, 12748–12752.

[36] T. Ishiyama, M. Murata, N. Miyaura, *J. Org. Chem.* **1995**, *60*, 7508–7510.

[37] W. Li, D. P. Nelson, M. S. Jensen, R. S. Hoerrner, D. Cai, R. D. Larsen, P. J. Reider, *J. Org. Chem.* **2002**, *67*, 5394–5397.

[38] J. Tydlitát, S. Achelle, J. Rodríguez-López, O. Pytela, T. Mikýsek, N. Cabon, F. Robin-le Guen, D. Miklík, Z. Růžičková, F. Bureš, *Dyes Pigm.* **2017**, *146*, 467–478.

[39] J. Du, G. Hua, P. Beier, A. M. Z. Slawin, J. D. Woollins, *Struct. Chem.* **2017**, *28*, 723–733.

[40] C. Dehu, F. Meyers, J. L. Bredas, *J. Am. Chem. Soc.* **1993**, *115*, 6198–6206.

[41] C. W. Bird, *Tetrahedron* **1986**, *42*, 89–92.

[42] T. M. Krygowski, H. Szatylowicz, O. A. Stasyuk, J. Dominikowska, M. Palusiak, *Chem. Rev.* **2014**, *114*, 6383–6422.

[43] P. Liebing, C. R. Pitts, M. Reimann, N. Trapp, D. Rombach, D. Bornemann, M. Kaupp, A. Togni, *Chem. Eur. J.* **2021**, *27*, 6086–6093.

[44] M. Klikar, I. V. Kityk, D. Kulwas, T. Mikysek, O. Pytela, F. Bureš, *New J. Chem.* **2017**, *41*, 1459.

[45] A. K. Pal, A. F. Henwood, D. B. Cordes, A. M. Z. Slawin, I. D. W. Samuel, E. Zysman-Colman, *Inorg. Chem.* **2017**, *56*, 7533–7544.

[46] N. M. Shavaleev, G. Xie, S. Varghese, D. B. Cordes, A. M. Z. Slawin, C. Momblona, E. Ortí, H. J. Bolink, I. D. W. Samuel, E. Zysman-Colman, *Inorg. Chem.* **2015**, *54*, 5907–5914.

[47] F. Bureš, *RSC Adv.* **2014**, *4*, 58826–58851.

[48] M. J. Frisch, G. W. Trucks, H. B. Schlegel, G. E. Scuseria, M. A. Robb, J. R. Cheeseman, G. Scalmani, V. Barone, G. A. Petersson, H. Nakatsuji, X. Li, M. Caricato, A. V. Marenich, J. Bloino, B. G. Janesko, R. Gomperts, B. Mennucci, H. P. Hratchian, J. V. Ortiz, A. F. Izmaylov, J. L. Sonnenberg, D. Williams-Young, F. Ding, F. Lipparini, F. Egidi, J. Goings, B. Peng, A. Petrone, T. Henderson, D. Ranasinghe, V. G. Zakrzewski, J. Gao, N. Rega, G. Zheng, W. Liang, M. Hada, M. Ehara, K. Toyota, R. Fukuda, J. Hasegawa, M. Ishida, T. Nakajima, Y. Honda, O. Kitao, H. Nakai, T. Vreven, K. Throssell, J. A. Montgomery Jr., J. E. Peralta, F. Ogliaro, M. J. Bearpark, J. J. Heyd, E. N. Brothers, K. N. Kudin, V. N. Staroverov, T. A. Keith, R. Kobayashi, J. Normand, K. Raghavachari, A. P. Rendell, J. C. Burant, S. S. Iyengar, J. Tomasi, M. Cossi, J. M. Millam, M. Klene, C. Adamo, R. Cammi, J. W. Ochterski, R. L. Martin, K. Morokuma, O. Farkas, J. B. Foresman, D. J. Fox, **2016**.

[49] T. J. Carter, R. Mohtadi, T. S. Arthur, F. Mizuno, R. Zhang, S. Shirai, J. W. Kampf, *Angew. Chem., Int. Ed.* **2014**, *53*, 3173–3177.

[50] A. A. Isse, A. Gennaro, *J. Phys. Chem. B* **2010**, *114*, 7894–7899.

[51] D. T. Sawyer, A. Sobkowiak, J. L. Roberts, D. T. Sawyer, *Electrochemistry for Chemists*, Wiley, New York, **1995**.

[52] A. M. Brouwer, *Pure Appl. Chem.* **2011**, *83*, 2213–2228.

[53] D. Cvejn, E. Michail, K. Seintis, M. Klikar, O. Pytela, T. Mikysek, N. Almonasy, M. Ludwig, V. Giannetas, M. Fakis, F. Bureš, *RSC Adv.* **2016**, *6*, 12819–12828.

[54] Y. Gong, X. Guo, S. Wang, H. Su, A. Xia, Q. He, F. Bai, *J. Phys. Chem. A* **2007**, *111*, 5806–5812.

[55] F. Chen, W. Zhang, T. Tian, B. Bai, H. Wang, M. Li, *J. Phys. Chem. A* **2017**, *121*, 8399–8407.

[56] P. Gautam, Y. Wang, G. Zhang, H. Sun, J. M. W. Chan, *Chem. Mater.* **2018**, *30*, 7055–7066.

[57] V. Maffeis, R. Brisse, V. Labet, B. Jousselme, T. Gustavsson, *J. Phys. Chem. A* **2018**, *122*, 5533–5544.

[58] T. Jang, S. Lee, S. Park, H. Lee, Y. Pang, *J. Mol. Liq.* **2024**, *412*, 125791.

[59] W. Xu, L. Wei, Z. Wang, R. Zhu, J. Jiang, H. Liu, J. Du, T.-C. Weng, Y.-B. Zhang, Y. Huang, W. Liu, *J. Phys. Chem. B* **2021**, *125*, 10796–10804.

[60] S. Cao, H. Li, Z. Zhao, S. Zhang, J. Chen, J. Xu, J. R. Knutson, L. Brand, *Molecules* **2021**, *26*, 211.

[61] L. Martinez-Fernandez, T. Gustavsson, U. Diederichsen, R. Improta, *Molecules* **2020**, *25*, 824.

[62] S. G. Bairu, E. Mghanga, J. Hasan, S. Kola, V. J. Rao, K. Bhanuprakash, L. Giribabu, G. P. Wiederrecht, R. da Silva, L. G. C. Rego, G. Ramakrishna, *J. Phys. Chem. C* **2013**, *117*, 4824–4835.

[63] M. L. Horng, J. A. Gardecki, A. Papazyan, M. Maroncelli, *J. Phys. Chem.* **1995**, *99*, 17311–17337.

[64] P. K. Singh, S. Nath, M. Kumbhakar, A. C. Bhasikuttan, H. Pal, *J. Phys. Chem. A* **2008**, *112*, 5598–5603.

[65] O. Varnavski, X. Yan, O. Mongin, M. Blanchard-Desce, T. Goodson, *J. Phys. Chem. C* **2007**, *111*, 149–162.

[66] Y. Wang, G. S. He, P. N. Prasad, T. Goodson, *J. Am. Chem. Soc.* **2005**, *127*, 10128–10129.

[67] N. A. Montgomery, G. J. Hedley, A. Ruseckas, J.-C. Denis, S. Schumacher, A. L. Kanibolotsky, P. J. Skabara, I. Galbraith, G. A. Turnbull, I. D. W. Samuel, *Phys. Chem. Chem. Phys.* **2012**, *14*, 9176–9184.

[68] C. Liu, K.-C. Tang, H. Zhang, H.-A. Pan, J. Hua, B. Li, P.-T. Chou, *J. Phys. Chem. A* **2012**, *116*, 12339–12348.

[69] L. Yan, X. Chen, Q. He, Y. Wang, X. Wang, Q. Guo, F. Bai, A. Xia, D. Aumiler, S. Vdović, S. Lin, *J. Phys. Chem. A* **2012**, *116*, 8693–8705.

[70] Y. Li, G. He, X. Wang, Q. Guo, Y. Niu, A. Xia, *ChemPhysChem* **2016**, *17*, 406–411.

[71] V. Petropoulos, I. Georgoulis, C. Vourdaki, P. Hrobárik, I. Sigmundová, J. Nociarová, M. Maiuri, G. Cerullo, M. Fakis, *ChemPhysChem* **2023**, *24*, e202300127.

[72] M. Fakis, V. Petropoulos, P. Hrobárik, J. Nociarová, P. Osuský, M. Maiuri, G. Cerullo, *J. Phys. Chem. B* **2022**, *126*, 8532–8543.

[73] P. Hrobárik, V. Hrobáriková, I. Sigmundová, P. Zahradník, M. Fakis, I. Polyzos, P. Persephonis, *J. Org. Chem.* **2011**, *76*, 8726–8736.

[74] N. S. Makarov, M. Drobizhev, A. Rebane, *Opt. Express* **2008**, *16*, 4029–4047.

[75] M. J. Plater, T. Jackson, *J. Chem. Soc., Perkin Trans. 1* **2001**, 2548–2552.

[76] Z. Otwinowski, W. Minor, in *Methods in Enzymology*, Academic Press, **1997**, pp. 307–326.

[77] F. R. Ahmed, S. R. Hall, C. P. Huber, International Union of Crystallography, Carleton University, Eds. *Crystallographic Computing: Proceedings of an International Summer School Organized by The Commission on Crystallographic Computing of the International Union of Crystallography and Held in Ottawa, 4-11 August 1969*, Munksgaard, Copenhagen, **1970**.

[78] A. Altomare, G. Cascarano, C. Giacovazzo, A. Guagliardi, *J. Appl. Crystallogr.* **1994**, *27*, 1045–1050.

[79] G. M. Sheldrick, *Acta Crystallogr., Sect. C:Struct. Chem.* **2015**, *71*, 3–8.